RESEARCH ARTICLE | MAY 21 2018

Linear response approach to active Brownian particles in time-varying activity fields

Holger Merlitz ; Hidde D. Vuijk; Joseph Brader; Abhinav Sharma; Jens-Uwe Sommer

J. Chem. Phys. 148, 194116 (2018)
https://doi.org/10.1063/1.5025760

Linear response approach to active Brownian particles in time-varying activity fields

Holger Merlitz,[1,a)] Hidde D. Vuijk,[1] Joseph Brader,[2] Abhinav Sharma,[1] and Jens-Uwe Sommer[1,3]
[1]*Leibniz-Institut für Polymerforschung Dresden, Institut Theorie der Polymere, 01069 Dresden, Germany*
[2]*Department of Physics, University of Fribourg, CH-1700 Fribourg, Switzerland*
[3]*Technische Universität Dresden, Institute of Theoretical Physics, 01069 Dresden, Germany*

(Received 13 February 2018; accepted 3 May 2018; published online 21 May 2018)

In a theoretical and simulation study, active Brownian particles (ABPs) in three-dimensional bulk systems are exposed to time-varying sinusoidal activity waves that are running through the system. A linear response (Green-Kubo) formalism is applied to derive fully analytical expressions for the torque-free polarization profiles of non-interacting particles. The activity waves induce fluxes that strongly depend on the particle size and may be employed to de-mix mixtures of ABPs or to drive the particles into selected areas of the system. Three-dimensional Langevin dynamics simulations are carried out to verify the accuracy of the linear response formalism, which is shown to work best when the particles are small (i.e., highly Brownian) or operating at low activity levels. *Published by AIP Publishing.* https://doi.org/10.1063/1.5025760

I. INTRODUCTION

Biological systems often contain microscopic objects of different sizes featuring a self-propulsion to play a crucial role in vital actions. Prominent examples are white blood cells chasing intruders,[1] motor proteins facilitating the transport of, e.g., RNA inside cells,[2] or bacteria such as *Escherichia coli* which are simply searching for food.[3]

On the other hand, synthetic micro-swimmers are designed to offer hope-bearing solutions to problems that are hard to approach with the toolbox available to conventional nanotechnology.[4,5] Potential fields of applications are highly directional drug delivery, improved bio-markers or contrast agents,[6] and the elimination of pollutants in the framework of environmental protection.[7]

By far the simplest synthetic self-propelling agents are binary Janus particles of spherical shape. These particles may be driven by catalytic reactions with an ingredient of the solvent such as hydrogen peroxide[8] or hydrazine.[9] If the "fuel" exhibits a concentration gradient, then the activity of these active Brownian particles (ABPs) turns position dependent, leading to phenomena that have recently been demonstrated to resemble chemotaxis.[10–12] Instead of being chemically driven, Janus particles may also respond to light as a result of inhomogeneous surface heating and the resulting local temperature gradient.[13] This resembles phototactic behavior, and since light intensities are easily controlled in a laboratory setup, not only positions but also rapidly varying time-dependent activity profiles may be employed to manipulate ABPs. Recent reviews about the state of the art of artificial nanomotors have been presented by Yamamoto and Shioi[5] and Bechinger *et al.*[14]

Some of the authors have recently applied the linear response (Green-Kubo) approach to ABPs and successfully computed average swim speeds[15] in homogeneous systems as well as a torque-free polarization and the resulting density distributions in systems with spatially inhomogeneous activity profiles.[16] In the present work, we generalize that formalism to systems of non-interacting particles in which the activity fields are additionally time dependent. Recently, Geiseler *et al.* have analyzed the behavior of micro-swimmers in active density waves that are sweeping over the ABPs and thereby driving them into selected directions.[17,18] Techniques to manipulate the global direction of motion of ABPs are naturally of paramount interest to the practitioner. While existing studies are restricted to two-dimensional setups and thus affected by boundary effects of the substrate on which the particles are sliding, our linear response approach is going to be applied to three-dimensional bulk systems in the absence of boundaries.

In Sec. II, we first present our model, the system of units, and a short introduction to linear response theory. Section III derives the orientation profiles of ABPs that are exposed to a propagating sinusoidal activity wave. The resulting torque-free polarization profiles inside the activity gradient are derived as a fully analytical expression and compared to Langevin dynamics simulations. These profiles are functions of the key parameters of the activity wave such as its phase velocity and wave number. The corresponding density distributions are derived in Sec. IV and again a close agreement with the simulations is reported. Section V studies the fluxes induced into the ABPs by the propagating activity wave, which strongly depend on the particle size. This fact is exploited in Sec. VI in which a mixture of ABPs of different sizes is de-mixed by selective applications of induced fluxes. We discuss the parameter ranges in which the linear response ansatz yields

[a)]merlitz@posteo.de

accurate predictions (Sec. VII) and summarize our findings in Sec. VIII.

II. MODEL AND THEORY

A. Numerical simulations

In this work, we introduce a standard particle with a diameter of $b = 1$ and mass $m = 1$, which defines the length and mass units. We explicitly specify the translational diffusion coefficient $D_t = k_B T/\zeta$ and the drag coefficient ζ, and with $k_B = 1$, the unit-less temperature of the system is specified, too. The unit time τ is the time which the standard particle needs to diffuse over the distance of its diameter, i.e., $\tau = (6D_t)^{-1}$. We have thus scaled the remaining parameters to yield $\tau = 1$.

The Langevin dynamics simulations were carried out with the molecular dynamics simulation package Large-scale Atomic/Molecular Massively Parallel Simulator (LAMMPS)[19] in fully three-dimensional setups. The activity is induced by an explicit force that acts in the direction of the particle's internal orientation vector, and noise is induced by a Langevin thermostat at a system temperature of $T = 5/3$. We use an integration time step of $4{\cdot}10^{-4}$. In the simulations of Secs. III–V, 500 active particles are placed into a box of the size $L^3 = 15^3$ and periodic boundaries. The particles are not interacting, so that actually an ensemble of single particles is simulated. The results are therefore accurate for setups in which the density of ABPs remains low so that the influence of two-body interactions is negligible. In Sec. VI, particles of different diameters are distributed inside a larger box of size $15 \times 15 \times 150$, being bounded in the z-direction with impenetrable walls, but periodic in x- and y-directions. In this case, their diameters are given in multiples of the diameter of the standard particle, which continues to define all re-scaled units. Note that the simulations, unlike the theoretical approximations we are going to apply, are carried out using Langevin dynamics, for which key parameters like the frictional drag and diffusion coefficients have to be scaled individually with the diameter of each species. The resulting parameters for all particles are summarized in Table I. Further technical details regarding the implementation of ABPs in LAMMPS have been described in our previous publication.[20]

With the choice of parameters as above, the motion of an active particle is over-damped on the time scale of τ_r. In the over-damped limit, the motion of an active particle can be modeled by the Langevin equations

$$\dot{\boldsymbol{r}} = \frac{f(\boldsymbol{r},t)}{\zeta}\boldsymbol{p} + \boldsymbol{\gamma}, \quad \dot{\boldsymbol{p}} = \boldsymbol{\eta} \times \boldsymbol{p} \tag{1}$$

with coordinates $\boldsymbol{r}$ and the embedded unit vector $\boldsymbol{p}$ which defines the particle orientation. f is the modulus of the force that drives the particle into the direction of its orientation vector and ζ is the frictional drag coefficient. The stochastic vectors $\boldsymbol{\gamma}(t)$ and $\boldsymbol{\eta}(t)$ are Gaussian distributed with zero mean and time correlations $\langle \boldsymbol{\gamma}(t)\boldsymbol{\gamma}^T(t')\rangle = 2D_t \mathbb{1}\delta(t-t')$ and $\langle \boldsymbol{\eta}(t)\boldsymbol{\eta}^T(t')\rangle = 2D_r \mathbb{1}\delta(t-t')$, with the identity matrix $\mathbb{1}$ and the translational and rotational diffusion coefficients D_t and D_r, respectively. The latter is related to the rotational relaxation time according to $\tau_r = 1/(2D_r)$. Note that in the second part of Eq. (1), the orientation vector does not couple to the activity field and hence no direct torque acts on the particle due to the position-dependent activity. Our linear response, presented in Subsection II B, is based on the over-damped set of equations (1).

TABLE I. Simulation parameters for ABPs of different diameters b. The mass m is required for the integrator, but the resulting momentum relaxation time τ_m is significantly shorter than τ_r, and therefore, the motion of the particle is over-damped on the time scale of τ_r.

Diameter, b	0.5	1	2
Mass, m	1/8	1	8
Frictional drag coefficient, ζ	5	10	20
Momentum relaxation time, τ_m	1/40	1/10	2/5
Translational diffusion coefficient, D_t	1/3	1/6	1/12
Rotational diffusion coefficient, D_r	4	1/2	1/16
Rotational relaxation time, τ_r	1/8	1	8
Ratio, τ_r/τ_m	5	10	20

B. Linear response ansatz

It follows exactly from (1) that the joint N-particle probability distribution $P(t) \equiv P(\boldsymbol{r}^N, \boldsymbol{p}^N, t)$ evolves according to[21]

$$\frac{\partial P(t)}{\partial t} = \Omega_a(t)P(t) \tag{2}$$

with the time-evolution operator Ω_a. The time-evolution operator can be split into a sum of two terms, $\Omega_a(t) = \Omega_{\rm eq} + \delta\Omega_a(t)$, where the equilibrium contribution is given by

$$\Omega_{\rm eq} = \sum_{i=1}^{N} \boldsymbol{\nabla}_i \cdot \left[D_{\rm t}(\boldsymbol{\nabla}_i - \beta \boldsymbol{F}_i)\right] + D_{\rm r}\boldsymbol{R}_i^2, \tag{3}$$

with the rotation operator $\boldsymbol{R} = \boldsymbol{p} \times \nabla_{\boldsymbol{p}}$,[22] $\beta = 1/(k_{\rm B}T)$, and an external force $\boldsymbol{F}_i$. The active part of the dynamics is described by the operator $\delta\Omega_a = -\sum_i \boldsymbol{\nabla}_i \cdot (v_0(\boldsymbol{r}_i,t)\boldsymbol{p}_i)$. We refer to Refs. 15 and 16 for a detailed elaboration of the linear response formalism. Here, we only give a brief outline of the method. We obtain from Eq. (2) an exact expression for the non-equilibrium average of a test function $g \equiv g(\boldsymbol{r}^N, \boldsymbol{p}^N)$ as

$$\langle g\rangle(t) = \langle g\rangle_{\rm eq} - \int_{-\infty}^{t} dt' \, \langle G(t') e_{-}^{\int_{t'}^{t} ds\, \Omega_a^{\dagger}(s)} g\rangle_{\rm eq}, \tag{4}$$

where e_- is a negatively ordered exponential function.[23] We have defined $G(t) = K(t) + V(t)$ with

$$K(t) = \sum_{i=1}^{N} v_0(\boldsymbol{r}_i,t)\boldsymbol{p}_i \cdot \beta \boldsymbol{F}_i, \tag{5}$$

$$V(t) = \sum_{i=1}^{N} \boldsymbol{p}_i \cdot \nabla_i v_0(\boldsymbol{r}_i,t), \tag{6}$$

in which v_0 corresponds to the driven velocity of the particle, related to the driving force via $v_0 = f/\zeta$ on time scales that are large compared to the momentum relaxation time τ_m. The adjoint operator is given by $\Omega_a^{\dagger}(t) = \Omega_{\rm eq}^{\dagger} - \delta\Omega_a(t)$, where $\Omega_{\rm eq}^{\dagger} = \sum_i D_t(\boldsymbol{\nabla}_i + \beta \boldsymbol{F}_i) \cdot \boldsymbol{\nabla}_i + D_r \boldsymbol{R}_i^2$, with $\boldsymbol{F}_i = 0$ in what follows. Linear response corresponds to the system response when the full-time evolution operator in (4) is replaced by the time-independent equilibrium adjoint operator. This

is equivalent to assuming that the active system is close to the equilibrium and the activity corresponds to a small perturbation.

III. POLARIZATION IN THE ACTIVITY FIELD

The activity field is a time-dependent function of the z-coordinate, which defines the modulus of the driving force of Eq. (1) as

$$f(z,t) = f_0\{\sin[k(z-vt)] + s\}, \tag{7}$$

with the factor $f_0 = 2.5$, the system time t, the phase velocity v, and the shift $s = 1.0$. A vertical shift of $s \geq 1$ is required to avoid unphysical negative values for the activity. Simulations require finite box-sizes, and to avoid boundary effects, the box is equipped with periodic boundaries, which enforce discretized wave numbers

$$k = \frac{2n\pi}{L}, \tag{8}$$

with the box-length L and positive integers n. The average orientation per particle is defined as

$$\boldsymbol{p}(\boldsymbol{r}) = \frac{\langle \sum_i \delta(\boldsymbol{r}-\boldsymbol{r}_i)\boldsymbol{p}_i\rangle}{\rho(\boldsymbol{r})}, \tag{9}$$

with the one-body density $\rho(\boldsymbol{r}) = \langle \sum_i \delta(\boldsymbol{r}-\boldsymbol{r}_i)\rangle$. The steady-state average orientation corresponding to a time-independent inhomogeneous activity field has been already obtained in Ref. 16. Corresponding to a space- and time-dependent activity, the steady-state orientation can be obtained using Eq. (4) as

$$\boldsymbol{p}(\boldsymbol{r},t) = \int_{-\infty}^{t} dt' \int d\boldsymbol{r}' v_0(\boldsymbol{r}',t')\, \chi(|\boldsymbol{r}-\boldsymbol{r}'|, |t-t'|), \tag{10}$$

where the space-time response function, $\chi(|\boldsymbol{r}-\boldsymbol{r}'|, |t-t'|)$, is given by

$$\chi(|\boldsymbol{r}-\boldsymbol{r}'|, |t-t'|) = \frac{e^{-2D_r|(t-t')|}}{3} \nabla G^s_{\mathrm{VH}}(|\boldsymbol{r}-\boldsymbol{r}'|, |t-t'|). \tag{11}$$

In Eq. (11), $G_{\mathrm{VH}}(r,\, t)$ corresponds to the self-part of the Van Hove function. This function can be approximated as a Gaussian[24]

$$G^s_{\mathrm{VH}}(\boldsymbol{r},t) = \frac{1}{(4\pi D_t t)^{3/2}}\, e^{-r^2/4D_t t}. \tag{12}$$

We note that this approximation is valid even in the case of interacting particles for any spherically-symmetric interaction potential, provided the density is sufficiently low.[16] Therefore, the presented result is a generic one and not limited to ideal gases. In this work, we have considered non-interacting particles as a special case, for which the Gaussian approximation for the Van Hove function is exact.

Using Eqs. (10) and (11), the average orientation corresponding to the activity wave in Eq. (7) is obtained as

$$p(z,t) = -\frac{f_0\, k}{3\zeta} \int_0^\infty dt' \int_{-\infty}^\infty dz'\, \cos\left[k(z'-v(t-t'))\right] \cdot \frac{\exp\left[-2D_r t' - \frac{(z-z')^2}{4D_t t'}\right]}{\sqrt{4\pi D_t t'}} \tag{13}$$

yielding

$$p(z,t) = -\frac{f_0\, k\cos\left[k(z-vt)+\psi\right]}{3\zeta\sqrt{(2D_r + D_t k^2)^2 + v^2}}, \tag{14}$$

where we have introduced the phase shift

$$\psi = \arctan\left[\frac{v}{2D_r + D_t k^2}\right]. \tag{15}$$

The walker's orientation, Eq. (14), is stationary in the comoving coordinate frame $\xi = z - vt$ and is shown in Fig. 1: With increasing phase velocity, the amplitude of the orientation is decreasing, while the phase shift increases. This is immediately obvious in Eq. (14), which exhibits the phase velocity in its denominator, and in Eq. (15) in which the phase shift increases linearly with v in its leading order Taylor term. With increasing phase velocity of the activity wave, the activity changes rapidly so that the particle is eventually unable to respond to changes of the external field. The crucial time scale is the rotational relaxation time τ_r, and when the activity wave runs from its minimum to its next maximum during that time, the orientation profile essentially turns flat. This happens at phase velocities of the order of $|v| \approx \pi/k\tau_r$. As a function of the wave number k, the amplitude of the orientation, $f_0\, k/(3\zeta\sqrt{(2D_r + D_t k^2)^2 + v^2})$, has a maximum at

$$\tilde{k} = \sqrt{\frac{v^2}{3D_t\zeta} + \frac{2D_r}{D_t}}, \tag{16}$$

while the phase shift ψ is diminishing with increasing values of k. The orientation is generally pointing against the activity gradient: i.e., the ABP is turning toward the direction in which activity decreases.[16]

The linear response theory generally overestimates the degree of orientation, as well as the amount of phase shift. The deviation from the simulation results increases with the magnitude of the driving force, or the pre-factor f_0 in Eq. (7). On the other hand, we have observed almost perfect agreement with the simulation data when f_0 was set smaller than 0.1. It is clear that the validity of the linear response approximation remains restricted to the regime of low activities.

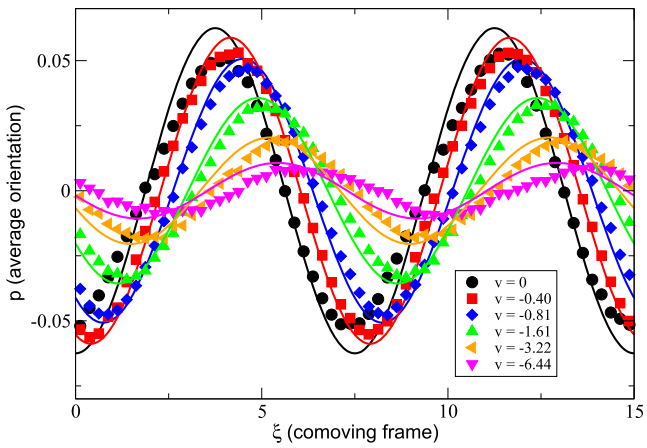

FIG. 1. Average orientation of the ABP in the coordinate system which moves with the phase velocity v of the activity wave. Symbols are MD simulations and closed curves are the approximation Eq. (14). In this example, $b = 1$, $k = 0.84$, $f_0 = 2.5$, and $s = 1$.

IV. DENSITY DISTRIBUTIONS

Traveling activity waves as in Eq. (7) induce traveling orientation waves [Eq. (14)] and traveling density waves. One cannot, however, use the linear response approach to calculate the density distribution because it is invariant to the activity in linear order. To calculate the density distribution, we take Eq. (2) in the single-particle limit and integrate over $\boldsymbol{p}$, x, and y in Eq. (2) to obtain the following 1-dimensional equation for the density $\rho(z, t)$:

$$\frac{\partial \rho(z,t)}{\partial t} = \frac{\partial}{\partial z}\left[D_t \frac{\partial \rho(z,t)}{\partial z} - \frac{f_0(z,t)}{\zeta} p(z,t)\rho(z,t)\right]. \quad (17)$$

In the comoving frame ξ, Eq. (17) can be recast as a continuity equation

$$\frac{\partial \rho}{\partial t} + \frac{\partial J}{\partial \xi} = 0, \quad (18)$$

where $\rho = \rho(z - vt) \equiv \rho(\xi)$ and $J(\xi)$ is the flux in the comoving frame given as

$$J(\xi) = -D_t \frac{\partial \rho}{\partial \xi} + \frac{f(\xi)}{\zeta} p(\xi)\,\rho(\xi) - v\,\rho(\xi). \quad (19)$$

Since the density is stationary in the ξ-frame, it follows from Eq. (18) that $J(\xi)$ is constant. On integrating Eq. (19) and using the periodicity of $p(\xi)$ and $\rho(\xi)$, one obtains the following equations for the flux:

$$\frac{J}{\rho_b L D_t} = \frac{\left[1 - \exp\left\{-\int_0^L \frac{b(z)}{D_t}\,dz\right\}\right]}{\int_0^L dx \int_0^L dy \exp\left\{-\int_x^{x+y} \frac{b(z)}{D_t}\,dz\right\}} \quad (20)$$

and the density

$$\frac{\rho(\xi)}{\rho_b} = \frac{L \int_0^L dy \exp\left[-\int_\xi^{\xi+y} \frac{b(\xi')}{D_t}\,d\xi'\right]}{\int_0^L dy' \int_0^L dy \exp\left[-\int_{y'}^{y'+y} \frac{b(\xi')}{D_t}\,d\xi'\right]}, \quad (21)$$

with the particle bulk density $\rho_b = N/V$ and the function $b(\xi) = \zeta^{-1} f(\xi)\, p(\xi) - v$. We remind once again that these distributions refer to single particle ensembles, and that interactions between particles are not accounted for. They turn inaccurate as soon as particle densities reach levels at which the two-body virial coefficient contributes significantly to the free energy of the system.

This integral [Eq. (21)] has to be solved numerically, and solutions are shown in Fig. 2. We have used the theoretical prediction of Eq. (14) for $p(\xi)$. The linear response theory offers an excellent approximation to the simulation data in the present parameter ranges. A comparison to Fig. 1 reveals the different time scales at which the variables respond to the activity field: While the density distribution is almost uniform at phase velocities as low as $|v| \approx 1.6$, the polarization pattern is not yet flat at a far higher velocity of $|v| \approx 6.4$. This is a consequence of the longer relaxation times associated with translocations of the ABPs, as compared to their rotational relaxation times. In the present parameter setting, the particle positions relax roughly at an order of magnitude slower than their orientations.

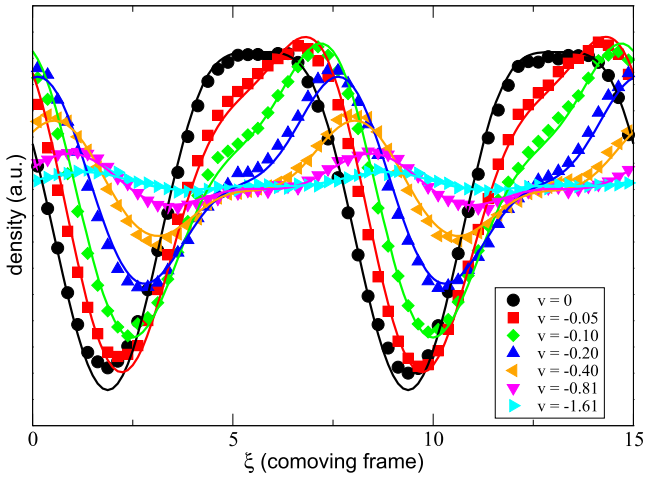

FIG. 2. Density distributions of the ABPs in the coordinate comoving frame at different phase velocities of the activity wave. Symbols are MD simulations and closed curves are the approximation Eq. (21). In this example, $b = 1$, $n = 2$, $f_0 = 2.5$, and $s = 1$.

V. INDUCED FLUX

The average drift velocity of the ABPs in the laboratory frame can be written as

$$v_d = \frac{J}{\rho_b} + v. \quad (22)$$

Figure 3 displays solutions to Eq. (22) for different wave numbers $k = 2n\pi/L$ of the activity waves. As a function of the phase velocity, the induced drift generally exhibits a global maximum, which, however, differs with the wave number. The overall maximum value of the drift velocity is found with $n = 6$ and a phase velocity about $v \approx 0.75$. We note that an earlier study has reported on situations in which negative drifts, i.e., in the direction opposite to the propagation of the activity wave.[17,18] The setups invested in these studies were two-dimensional and included a coupling term between particles and substrate. So far, we have not been able to reproduce

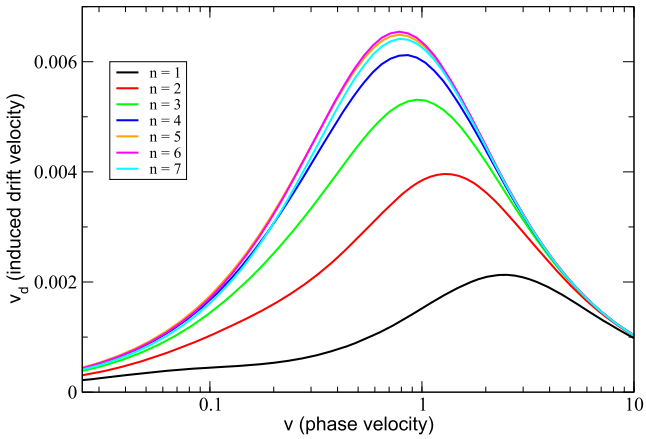

FIG. 3. Induced drift velocities [Eq. (22)], as a function of the phase velocity of the activity wave in a periodic simulation box of size L. Different curves correspond to different values of the wave numbers $k = 2n\pi/L$ which satisfy the periodic boundary condition. Here, the size of the ABP equals $b = 1$, and the activity factor $f_0 = 2.5$.

such a phenomenon with our setup in three dimensions, neither in linear response approximation nor in simulation. It may well be the case that the parameter range covered in our studies did not allow for such a reversal of the direction of drift. Furthermore, our system does not encompass any interactions between particles, between particles and substrates, nor any torques which would arise due to a non-spherical shape of the particle.

It is natural to ask how an induced drift would depend upon the properties of the particle. We have repeated the analysis of Fig. 3 with particles of sizes $b = 0.5$ and $b = 2$, with properties as summarized in Table I. Note that, since these particles are going to be mixed and exist simultaneously in the simulation box, no re-scaling of length units to the diameters of every particle species is possible. This implies that the standard-particle of size $b = 1$ continues to define the unit length, while the diameters of all other species are represented as multiples of diameters of the standard particle. Figure 4 only contains curves for wave numbers at which the respective particles reach the highest drift velocities. For small ABPs, MD simulations and linear response theory [Eq. (22)] display a reasonably close agreement. For the larger particle of diameter $b = 2$ (green curve and triangles), however, significant deviations are visible. Due to their longer rotational relaxation times, the dynamics of these particles are less affected by Brownian motion, i.e., more ballistic, and linear response theory begins to break down. In Sec. VII we are going to discuss the issue of validity ranges of the linear response approach in detail.

It is instructive to investigate an approximation to the induced drift velocity, considering that the orientation of the particle relaxes faster than its density profile. If the traveling wave propagates sufficiently fast, then the particles do not have sufficient time to re-arrange their locations within the time scale set by the oscillating activity wave, and $\rho(\xi)$ in Eq. (19) may be replaced with the uniform bulk density, turning Eq. (22) into

$$v_d(\xi) \approx \frac{1}{\zeta} p(\xi) f(\xi) \tag{23}$$

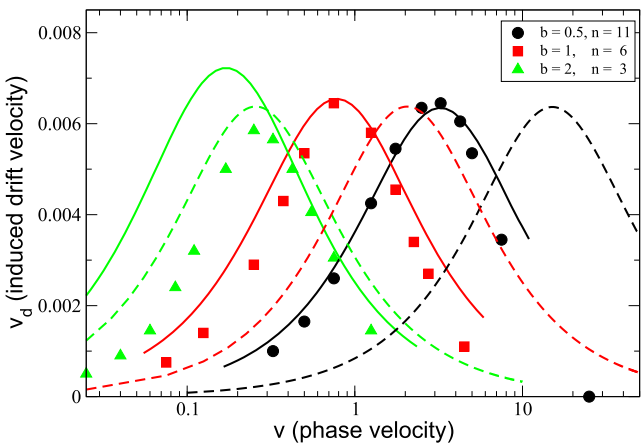

FIG. 4. Induced drift velocities as a function of the phase velocity, for different particle sizes and wave numbers $k = 2n\pi/L$, using $f_0 = 2.5$. Data points are simulations, solid curves are computed from Eq. (22), and dashed curves are the approximation (24).

which can be integrated over the box to yield the average drift velocity

$$v_d = \frac{f_0^2 k v}{6\zeta^2[(2D_r + D_t k^2)^2 + v^2]}. \tag{24}$$

The plots in Fig. 4 show that this approximation (dashed curves) is reasonable only in case of the large particles, which display a sufficiently slow reaction to the incoming activity field so that $\rho(\xi) \approx \rho_b$ remains valid. Yet, Eq. (24) provides us with a glimpse of how the underlying dynamics of the ABPs enable the induction of drift: This function has its extremum at

$$\tilde{v} = 4D_r \sim b^{-3}, \quad \tilde{k} = \sqrt{\frac{2D_r}{D_t}} \sim b^{-1}, \tag{25}$$

at which it reaches the induced drift velocity of

$$v_{d,\max} = \frac{\sqrt{2}}{48} \frac{f_0^2}{\zeta^2 \sqrt{D_r D_t}} \sim b^0, \tag{26}$$

where we used the fact that $\zeta \sim b$. The optimum choice for the velocity of the traveling wave is determined by the rotational diffusion and thus strongly dependent on the particle size. While the b^{-3}-scaling of this approximation to the optimum drift velocity definitely overestimates the simulation results, for which the scaling is closer to b^{-2}, the ideal wave number is inversely proportional to b in both, approximation and simulation. The maximum drift velocity is not an explicit function of the particle size, which is as well supported by the simulations (Fig. 4) and thus no spurious consequence of the uniform-density approximation. In the laboratory, of course, the driving force f_0 is likely to depend on the particle diameter and in this way the maximum achievable drift velocities may turn species-dependent.

VI. SEPARATION OF MIXTURES OF ABPs WITH DIFFERENT SIZES

In this set of simulations, the box-length was increased to $L = 150$ in z-direction because a drift over longer distances allows for a superior separation between the particle species. The boundaries were fixed with short-range repulsive walls. Three particle species were added, 500 particles each, with parameters as summarized in Table I. No interactions between particles were enabled so that these are pure averages of single particle ensembles. Then, activity waves were sent through the system, with positive phase velocities (from the left to the right in Fig. 5) parameters at which the solid curves of Fig. 4, e.g., Eq. (22), had their maxima.

As can be seen in Fig. 5, the different values of induced drift velocities allow for a separation of the mixture of particle species: Either one of the three species may be enriched at the right hand wall, depending on the particular choice of the activity wave. It is therefore possible to separate a mixture of ABPs according to their diameter. In the present simulation, the density distributions of the enriched species had turned stationary after simulation times of roughly 10^4, so that a continuation of that procedure did not improve its selectivity any further. At $z = 150$, the densities are dropping, which is caused by the repulsion between the finite-sized particles and the container

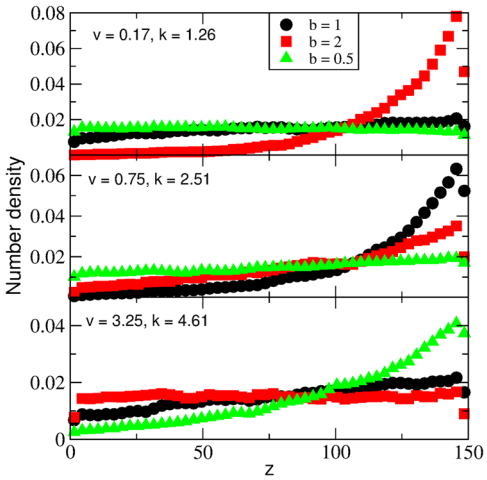

FIG. 5. A mixture of three ABP-species of different diameters. Depending on the choices for the phase velocity v and the wave number k of the activity wave, either the large particles (upper panel), the medium sized particles (center panel), or the small particles (lower panel) are enriched near the wall. The activity factor $f_0 = 2.5$ is the same for all particles. Note that the box-length is increased to $L = 150$ in this simulation.

wall. We want to remind that the present simulations contained non-interacting particles. In situations in which the volume fractions of ABPs turn high, as is partially the case when they become enriched at the fixed boundary, interactions between them are expected to turn relevant. These are not considered in the present study.

VII. VALIDITY OF THE LINEAR RESPONSE APPROACH

The solution to Eq. (2) is based on a separation of the time evolution operator $\Omega_a(t) = \Omega_{\rm eq} + \delta\Omega_a(t)$ into its (diffusive) equilibrium part and a second activity driven part, which is treated as a perturbation. This linear response ansatz produces accurate dynamics as long as diffusion dominates over driven motion.

To compare both components, we consider the persistence length of ballistic motion, $l_b = v_b\tau_r = f\tau_r/\zeta$, with the average diffusion distance $l_d = \sqrt{6D_t\tau_r}$ during the same time interval τ_r. As long as $l_b/l_d \ll 1$, diffusion dominates the motion. In our present simulations, the peak driving force reaches $f = 5$, at which $l_b/l_d = 1/4$ ($b = 1/2$), $l_b/l_d = 1/2$ ($b = 1$), and $l_b/l_d = 1$ ($b = 2$), which indicates that the formalism is likely to break down in case of the large particles, as is obvious in Fig. 4.

A diffusion driven dynamics is not uncommon for ABPs of the sub-100 nm scale. As an example, we consider the dynamics of Au–Pt Janus particles of diameter 30 nm, as prepared and analyzed by Lee *et al.*:[25] In a solution of water with 2.5% H_2O_2, these particles developed a considerable ballistic speed of $2.2\cdot10^4$ particle diameters per second. However, due to their small diameters, the rotational diffusion was rapid and allowed for a persistent motion over a distance of only $l_b \approx 4.6$ nm during the directional persistence time of $\tau_r \approx 7$ μs. Given the diffusion coefficient of the passive particle, $D_t \approx 0.013$ nm^2 ns^{-1}, the distance of $l_d = \sqrt{6D_t\tau_r} \approx 23$ nm was covered during one persistence time. This yields the ratio $l_b/l_d \approx 1/5$ so that linear response theory may safely be applied to this system.

We summarize that the linear response approximation describes ABPs at activity levels that are comparable or smaller than the diffusive motion of the particle and may hence be a method of choice for small ABPs of diameters in the sub-0.1 μm range, as well as for larger particles which are only weakly driven.

VIII. SUMMARY

In the present work, a linear response (Green-Kubo) approach has been applied to ABPs in three dimensions that are exposed to time-varying activity fields. We have demonstrated how activity gradients generate torque-free polarizations of the particles and evaluated analytically their orientation distributions. Density distributions and induced fluxes are derived and shown to agree closely with Langevin dynamics simulations within the range of validity of the formalism (Secs. III–V). Analytical results are discussed in certain limit cases.

The accuracy of linear response theory is granted as long as the dynamics of the ABPs is dominated by their thermal diffusive motion, while the active (driven) contribution remains weak. This is naturally the case with small ABPs of sub-100 nm diameter, or with larger particles that are only weakly driven (Sec. VII). The formalism presented here may be transferred to systems in two dimensions as well, provided that additional effects which arise from particle-substrate interactions are negligible or added to the equations.

Dynamic activity waves are capable of inducing fluxes into systems of ABPs, and the efficiency of that coupling is a function of the particle diameter, as is most easily verified in the approximation (25). A tuning of the phase velocity or wave number of the traveling wave allows the practitioner to efficiently drive particles of selected diameters through the system—a phenomenon, which might be applied to conduct a controlled separation of mixtures of ABPs according to their sizes (Sec. VI). Linear response theory allows us to determine the parameter sets which maximize the efficiency of the directional transport.

[1]G. Fenteany and M. Glogauer, Curr. Opin. Hematol. **11**, 15 (2004).
[2]Y. Kanai, N. Dohmae, and N. Hirokawa, Neuron **43**, 513 (2004).
[3]H. C. Berg, *E. Coli in Motion* (Springer Verlag, Heidelberg, Germany, 2004).
[4]S. J. Ebbens and J. R. Howse, Soft Matter **6**, 726 (2010).
[5]D. Yamamoto and A. Shioi, KONA Powder Part. J. **32**, 2 (2015).
[6]L. K. E. A. Abdelmohsen, F. Peng, Y. Tu, and D. A. Wilson, J. Mater. Chem. B **2**, 2395 (2014).
[7]W. Gao and J. Wang, ACS Nano **8**, 3170 (2014).
[8]J. R. Howse, R. A. L. Jones, A. J. Ryan, T. Gough, R. Vafabakhsh, and R. Golestanian, Phys. Rev. Lett. **99**, 048102 (2007).
[9]W. Gao, A. Pei, R. Dong, and J. Wang, J. Am. Chem. Soc. **136**, 2276 (2014).
[10]F. Peng, Y. Tu, J. C. M. van Hest, and D. A. Wilson, Angew. Chem. **127**, 11828 (2015).
[11]P. K. Ghosh, Y. Li, F. Marchesoni, and F. Nori, Phys. Rev. E **92**, 012114 (2015).
[12]H. D. Vuijk, A. Sharma, D. Mondal, J.-U. Sommer, and H. Merlitz, Phys. Rev. E **97**, 042612 (2018).
[13]C. Lozano, B. ten Hagen, H. Löwen, and C. Bechinger, Nat. Commun. **7**, 12828 (2016).

[14]C. Bechinger, R. D. Leonardo, H. Löwen, C. Reichhardt, G. Volpe, and G. Volpe, Rev. Mod. Phys. **88**, 045006 (2016).
[15]A. Sharma and J. Brader, J. Chem. Phys. **145**, 161101 (2016).
[16]A. Sharma and J. Brader, Phys. Rev. E **96**, 032604 (2017).
[17]A. Geiseler, P. Hänggi, F. Marchesoni, C. Mulhern, and S. Savel'ev, Phys. Rev. E **94**, 012613 (2016).
[18]A. Geiseler, P. Hänggi, and F. Marchesoni, Sci. Rep. **7**, 41884 (2017).
[19]S. Plimpton, J. Comput. Phys. **117**, 1 (1995), http://lammps.sandia.gov/.
[20]H. Merlitz, C. Wu, and J.-U. Sommer, Soft Matter **13**, 3726 (2017).
[21]C. W. Gardiner, *Stochastic Methods of Theoretical Physics* (Springer, Berlin, 1985), Vol. 3.
[22]P. M. Morse, H. Feshbach *et al.*, *Methods of Theoretical Physics* (McGraw-Hill, New York, 1953), Vol. 1.
[23]J. M. Brader, M. E. Cates, and M. Fuchs, Phys. Rev. E **86**, 021403 (2012).
[24]J.-P. Hansen and I. McDonald, *Theory of Simple Liquids* (Elsevier, New York, 1990), Vol. 3.
[25]T.-C. Lee, M. Alarcon-Correa, C. Mikch, K. Hahn, J. F. Gibbs, and P. Fischer, Nano Lett. **14**, 2407 (2014).